# Effects of spin-orbit coupling on quantum transport
Bardarson, J.H.

**Citation**
Bardarson, J. H. (2008, June 4). *Effects of spin-orbit coupling on quantum transport*. *Casimir PhD Series*. Retrieved from https://hdl.handle.net/1887/12930

# Chapter 4

# Degradation of Electron-Hole Entanglement by Spin-Orbit Coupling

## 4.1 Introduction

Spin-orbit coupling is one of the sources of degradation of spin entanglement that has been extensively investigated for electron pairs confined to two quantum dots [75]. In that context the spin-orbit coupling induces dephasing by coupling the electron spins via the orbital motion to fluctuating electric fields in the environment (due to lattice vibrations or gate voltage fluctuations). The coupling of the spins to the environment is needed for entanglement degradation because the spin-orbit coupling by itself amounts to a local unitary transformation of the electron states in the two quantum dots, which cannot change the degree of entanglement.

The characteristic feature of these quantum dots is that they are single-channel conductors with a conductance $G$ that is small compared to the conductance quantum $e^2/\hbar$. This implies in particular that the width of the energy levels is much smaller than the mean level spacing. At low voltages and temperatures there is then only a single accessible orbital mode. This is the main reason that spin-orbit coupling by itself cannot degrade the spin entanglement.
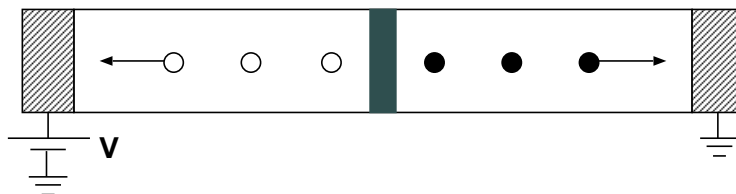
**Figure 4.1.** Multi-channel conductor containing a tunnel barrier. The applied voltage creates electron-hole pairs (solid and open circles) at opposite side of the barrier, whose spin state is maximally entangled. As the pair moves through the leads, the spin and orbital degrees of freedom become entangled by the spin-orbit coupling, degrading the spin entanglement upon tracing out the orbital degrees of freedom.

In a multi-channel conductor the situation is altogether different. Flying qubits in a multi-channel conductor can lose their entanglement as a result of spin-orbit coupling even in the absence of electric field fluctuations, because the large number of orbital degrees of freedom can play the role of an environment. This mechanism is the electronic analog of the loss of polarization entanglement by polarization-dependent scattering in quantum optics [76–78]. Fully-phase-coherent spin-orbit coupling can degrade the spin entanglement by reducing the pure spin state to a mixed spin density matrix — which typically has less entanglement than the pure state. Here we investigate this mechanism in the context of electron-hole entanglement in the Fermi sea [27]. Apart from the practical significance for the observability of the entanglement, this study provides a test for a theory of entanglement transfer based on the "isotropy approximation" that the spin state has no preferential quantization axis.

The system we consider, a multi-channel conductor containing a tunnel barrier, is schematically depicted in Fig. 4.1. The applied voltage $V$ creates, at each tunnel event, a maximally entangled electron-hole pair [79]. Spin-orbit coupling in the leads entangles the spin and orbital degrees of freedom. The spin state (obtained by tracing out the orbital degrees of freedom) is degraded from a pure state to a mixed state. The degree of entanglement of the spin state decreases and can vanish for strong spin-orbit coupling. We consider two cases. In the first case the leads are diffusive

wires while in the second case we model the leads as two chaotic cavities. Although the first case is our primary interest, we include the second case in order to test our approximate analytical calculations against an exact numerical simulation of the spin kicked rotator (cf. chapter 2).

The outline of this chapter is as follows. In Sec. 4.2 we calculate the density matrix of the electron-hole pairs in the regime where the tunnel conductance $G_{\text{tunnel}}$ is $\ll e^2/h$. This is the regime in which the electron-hole pairs form well separated current pulses, so that their entanglement can be measured easily [27]. (For $G_{\text{tunnel}} \gtrsim e^2/h$ different electron-hole pairs overlap in time, complicating the detection of the entanglement.) From the density matrix we seek, in Sec. 4.3, the degree of entanglement as measured by the concurrence [80]. For our analytical treatment we approximate the density matrix by the spin-isotropic Werner state [81]. The absence of a preferential basis in spin space is a natural assumption for a disordered or chaotic system, but it needs to be tested. For that purpose we use the spin kicked rotator, which as explained in Ch. 2 is a stroboscopic model of a chaotic cavity. We conclude in Sec. 4.4.

## 4.2  Calculation of the Electron-Hole State

### 4.2.1  Incoming and Outgoing States

Since the scattering of both orbital and spin degrees of freedom is elastic, we may consider separately each energy $E$ in the range $(E_{\text{F}}, E_{\text{F}} + eV)$. For ease of notation we will omit the energy arguments in what follows. We assume zero temperature, so the incoming state is

$$|\Psi_{\text{in}}\rangle = \prod_{\nu=1}^{2N} a_{L,\nu}^{\dagger} |0\rangle. \tag{4.1}$$

The creation operators $a_{L,\nu}^{\dagger}$, $\nu = 1, \ldots, 2N$ (acting on the true vacuum $|0\rangle$) occupy the $\nu$-th channel incoming from the left. The index $\nu$ labels both the $N$ orbital and two spin degrees of freedom. The $2N$ channels incoming from the right (creation operators $a_{R,\nu}^{\dagger}$) are unoccupied in the energy range $(E_{\text{F}}, E_{\text{F}} + eV)$. We collect the creation and annihilation operators

in vectors $\mathbf{a}_L = (a_{L,1}, a_{L,2}, \ldots, a_{L,2N})$, $\mathbf{a}_R = (a_{R,1}, a_{R,2}, \ldots, a_{R,2N})$.

The annihilation operators $b_{L,\nu}$ and $b_{R,\nu}$ of the outgoing channels are related to those of the incoming channels by the scattering matrix

$$\begin{pmatrix} \mathbf{b}_L \\ \mathbf{b}_R \end{pmatrix} = S \begin{pmatrix} \mathbf{a}_L \\ \mathbf{a}_R \end{pmatrix} = \begin{pmatrix} r & t' \\ t & r' \end{pmatrix} \begin{pmatrix} \mathbf{a}_L \\ \mathbf{a}_R \end{pmatrix}. \tag{4.2}$$

The $4N \times 4N$ unitary scattering matrix $S$ is decomposed into $2N \times 2N$ transmission and reflection matrices $t, t', r$, and $r'$. Substitution into Eq. (4.1) gives the outgoing state

$$|\Psi_{\text{out}}\rangle = \prod_{\nu=1}^{2N} \left( \sum_{\nu'=1}^{2N} \left[ b_{L,\nu'}^{\dagger} r_{\nu'\nu} + b_{R,\nu'}^{\dagger} t_{\nu'\nu} \right] \right) |0\rangle. \tag{4.3}$$

## 4.2.2   Tunneling Regime

We expand the outgoing state (4.3) in the small parameter $\epsilon = (h/e^2)G_{\text{tunnel}}$, neglecting terms of order $\epsilon$ and higher. Since $t, t'$ are $\mathcal{O}(\epsilon^{1/2})$ while $r, r'$ are $\mathcal{O}(\epsilon^0)$, we keep only terms linear in $t$ and $t'$. The result is

$$|\Psi_{\text{out}}\rangle = |0_{\text{F}}\rangle + \sum_{\nu,\mu} (tr^{\dagger})_{\nu\mu} b_{R,\nu}^{\dagger} b_{L,\mu} |0_{\text{F}}\rangle + \mathcal{O}(\epsilon), \tag{4.4}$$

where $|0_{\text{F}}\rangle$ is the unperturbed Fermi sea,

$$|0_{\text{F}}\rangle = \det(r) \prod_{\nu=1}^{2N} b_{L,\nu}^{\dagger} |0\rangle. \tag{4.5}$$

Since $rr^{\dagger} = \mathbb{1} - \mathcal{O}(\epsilon)$, we may assume that $r$ is a unitary matrix to the order in $\epsilon$ considered. The determinant $\det(r)$ is therefore simply a phase. The state (4.4) is a superposition of the unperturbed Fermi sea and a single electron-hole excitation, consisting of an electron in channel $\nu$ at the right and a hole in channel $\mu$ at the left.

As a check, we verify that the multi-channel result (4.4) reduces for

$N = 1$ to the single-channel result

$$\left| \Psi_{\text{out}}^{N=1} \right\rangle = |0_{\text{F}}\rangle + \frac{1}{\det(r)} \sum_{\nu,\mu} (t\sigma_2 r^T \sigma_2)_{\nu\mu} b_{R,\nu}^{\dagger} b_{L,\mu} |0_{\text{F}}\rangle + \mathcal{O}(\epsilon)$$

of Ref. 79. We use the identity [82]

$$\sigma_2 r^T \sigma_2 = \det(r) r^{\dagger}, \tag{4.6}$$

which holds for any $2 \times 2$ unitary matrix $r$ (with $\sigma_2$ a Pauli matrix). Hence $t\sigma_2 r^T \sigma_2 = \det(r)tr^{\dagger} + \mathcal{O}(\epsilon)$. Substitution into the single-channel result (4.6) indeed gives the multi-channel result (4.4) for $N = 1$.

### 4.2.3 Spin State of the Electron-Hole Pair

The spin state of the electron-hole pair is obtained from $|\Psi_{\text{out}}\rangle$ by projecting out the vacuum contribution and then tracing out the orbital degrees of freedom. This results in the $4 \times 4$ density matrix

$$\rho_{\alpha\beta,\gamma\delta} = \frac{1}{w} \sum_{n,m=1}^{N} (tr^{\dagger})_{n\alpha,m\beta} (tr^{\dagger})_{n\gamma,m\delta}^{*}, \tag{4.7}$$

with $w = \text{tr}(t^{\dagger} t r^{\dagger} r)$. Here $n$ and $m$ label the orbital degrees of freedom and $\alpha, \beta, \gamma$, and $\delta$ label the spin degrees of freedom.

We assume that the tunnel resistance is much larger than the resistance of the conductors at the left and right of the tunnel barrier. The transmission eigenvalues $T_n$ (eigenvalues of $tt^{\dagger}$) are then determined mainly by the tunnel barrier and will depend only weakly on the mode index $n$. We neglect this dependence entirely, so that $T_n = T$ for all $n$, the tunneling conductance being given by $G_{\text{tunnel}} = (2e^2/h)NT$.

To obtain a simpler form for the density matrix we use the polar decomposition of the scattering matrix

$$S = \begin{pmatrix} r & t' \\ t & r' \end{pmatrix} = \begin{pmatrix} u & 0 \\ 0 & v \end{pmatrix} \begin{pmatrix} \sqrt{1-\mathcal{T}} & \sqrt{\mathcal{T}} \\ \sqrt{\mathcal{T}} & -\sqrt{1-\mathcal{T}} \end{pmatrix} \begin{pmatrix} u' & 0 \\ 0 & v' \end{pmatrix}, \tag{4.8}$$

where $u$, $u'$, $v$, and $v'$ are unitary matrices and $\mathcal{T} = \text{diag}(T_1, T_2, \ldots, T_{2N})$.

For mode independent $T_n$'s the matrix $\mathcal{T}$ equals $T$ times the unit matrix. Hence

$$tr^\dagger = \sqrt{(1-T)T}\,U \tag{4.9}$$

is proportional to the $2N \times 2N$ unitary matrix $U = vu^\dagger$. Substitution into the expression (4.7) for the density matrix gives

$$\rho_{\alpha\beta,\gamma\delta} = \frac{1}{2N} \sum_{n,m=1}^{N} U_{n\alpha,m\beta} U^*_{n\gamma,m\delta}. \tag{4.10}$$

If there is no spin-orbit coupling, the matrix $U$ is diagonal in the spin indices: $U_{n\alpha,m\beta} = \tilde{U}_{nm}\delta_{\alpha\beta}$ with $\tilde{U}$ an $N \times N$ unitary matrix. The density matrix then represents the maximally entangled Bell state $|\psi_{\text{Bell}}\rangle$,

$$(\rho_{\text{Bell}})_{\alpha\beta,\gamma\delta} = \frac{1}{2}\delta_{\alpha\beta}\delta_{\gamma\delta} = |\psi_{\text{Bell}}\rangle\langle\psi_{\text{Bell}}|, \tag{4.11}$$

$$|\psi_{\text{Bell}}\rangle = \frac{1}{\sqrt{2}}\left(|\uparrow\rangle_e\,|\uparrow\rangle_h + |\downarrow\rangle_e\,|\downarrow\rangle_h\right), \tag{4.12}$$

with $|\sigma\rangle_{e,h}$ an electron ($e$) or hole ($h$) spin pointing up ($\sigma = \uparrow$) or down ($\sigma = \downarrow$). The state (4.11) is a pure state ($\rho^2_{\text{Bell}} = \rho_{\text{Bell}}$). Spin-orbit coupling will in general degrade $\rho$ to a mixed state, with less entanglement.

## 4.3   Entanglement of the Electron-Hole Pair

We quantify the degree of entanglement of the mixed electron-hole state (4.7) by means of the concurrence $C$ (which is in one-to-one correspondence with the entanglement of formation and varies from 0 for a nonentangled state to 1 for a maximally entangled state). Following Wootters [80] the concurrence is given by

$$C = \max\left\{0, \sqrt{\lambda_1} - \sqrt{\lambda_2} - \sqrt{\lambda_3} - \sqrt{\lambda_4}\right\}, \tag{4.13}$$

where the $\lambda_i$'s are the eigenvalues, in decreasing order, of the matrix product $\rho(\sigma_2 \otimes \sigma_2)\rho^*(\sigma_2 \otimes \sigma_2)$.

In the next two subsections we calculate the concurrence numerically for a chaotic cavity using Eq. (4.7) and analytically with an isotropy ap-

proximation for the density matrix.

### 4.3.1   Numerical Simulation

We calculate the concurrence $C$ numerically for the case that the scattering at the left and at the right of the tunnel barrier is chaotic. (The more experimentally relevant case of diffusive scattering will be considered in the next subsection.)

The total scattering matrix $S$ of the system (shown in Fig. 4.2) is constructed from the scattering matrix of the tunnel barrier,

$$S_T = \begin{pmatrix} \sqrt{1-T}\mathbb{1}_N & \sqrt{T}\mathbb{1}_N \\ \sqrt{T}\mathbb{1}_N & -\sqrt{1-T}\mathbb{1}_N \end{pmatrix}, \qquad (4.14)$$

and the scattering matrices $S_1$ and $S_2$ of the cavity on each side of the tunnel barrier. (We denote by $\mathbb{1}_N$ the $N \times N$ unit matrix.) We expand $S$ in the small parameter $T$ and keep terms up to order $\mathcal{O}(T^{1/2}) = \mathcal{O}(\epsilon^{1/2})$, consistent with the expansion of the outgoing state (4.4). This results in

$$r = r_1 + t_1' \frac{1}{1-r_1'} t_1 + \mathcal{O}(T), \qquad (4.15a)$$

$$t = t_2 \frac{1}{1+r_2} \sqrt{T} \frac{1}{1-r_1'} t_1 + \mathcal{O}(T^{3/2}), \qquad (4.15b)$$

and similar expressions for $r'$ and $t'$ which we do not need.

The scattering matrices $S_1$ and $S_2$ of the chaotic cavities are constructed from two spin kicked rotators. We briefly explain in Appendix 4.A how we use the results of chapter 2 to make a connection with the work in this chapter.

The resulting ensemble-averaged concurrence as a function of the ratio $\tau_{\mathrm{dwell}}/\tau_{\mathrm{so}}'$ of the mean dwell time $\tau_{\mathrm{dwell}}$ and spin-orbit coupling time $\tau_{\mathrm{so}}'$ is shown in Fig. 4.3. The dwell time $\tau_{\mathrm{dwell}}$ is the average time between a tunnel event and the escape of the particle into the left or right reservoir. The time $\tau_{\mathrm{so}}'$ is the exponential relaxation time of the spin-up and spin-down densities towards the equilibrium distribution[1]. (Both time scales

---

[1]In chapter 2 we calculate the spin relaxation time for spin amplitudes $\tau_{\mathrm{so}} = 2\tau_{\mathrm{so}}'$.
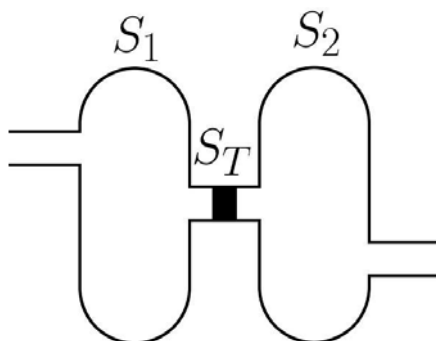
**Figure 4.2.** Two chaotic cavities with scattering matrices $S_1$ and $S_2$ connected by a tunnel barrier with scattering matrix $S_T$. The chaotic cavities are modeled by two spin kicked rotators.

are calculated in Appendixes 4.A and 4.B.) For a single channel, $N = 1$, the concurrence is unity independent of spin-orbit coupling strength since the trace over the orbital degrees of freedom leaves $\rho$ unchanged. From Fig. 4.3 (bottom panel) we see that for small $N$ the concurrence saturates at a nonzero value for large $\tau_{\mathrm{dwell}}/\tau'_{\mathrm{so}}$:

$$\lim_{\tau_{\mathrm{dwell}}/\tau'_{\mathrm{so}}\to\infty} \langle C \rangle = \begin{cases} 1, & N = 1, \\ 0.15, & N = 2, \\ 0.01, & N = 3. \end{cases} \tag{4.16}$$

The limiting value for $N = 2$ is close to that obtained in Ref. 83 in a single chaotic cavity. For $N \gtrsim 5$ the ensemble-averaged concurrence is negligible for large $\tau_{\mathrm{dwell}}/\tau'_{\mathrm{so}}$. The dependence of $\langle C \rangle$ on $\tau_{\mathrm{dwell}}/\tau'_{\mathrm{so}}$ becomes $N$ independent for $N \gtrsim 15$.

## 4.3.2　Isotropy Approximation

To obtain an analytical expression for the entanglement degradation we approximate the density matrix by the spin-isotropic Werner state [81]. The absence of a preferential basis in spin space means that the density
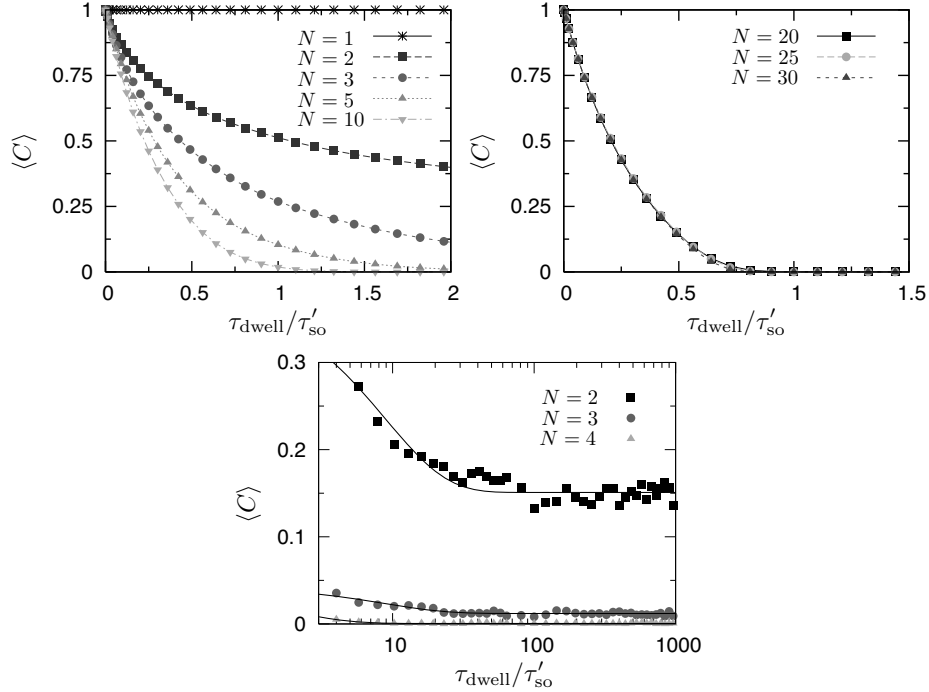
**Figure 4.3.** Ensemble averaged concurrence of the electron-hole pair scattered by two chaotic cavities, as a function of the spin-orbit coupling rate $1/\tau'_{\mathrm{so}}$ for different number of modes, $N$, in the leads. The data points are calculated from the spin kicked rotator; the lines are guides to the eye. The upper right panel shows that the results become $N$-independent for large $N$ while the bottom panel shows that for small $N$ the concurrence saturates at a finite value.

matrix $\rho$ for an electron-hole pair is invariant under the transformation

$$(V \otimes V^*)\rho(V^\dagger \otimes V^T) = \rho \qquad (4.17)$$

for all $2 \times 2$ unitary matrices $V$. This transformation rotates the spin basis of the electron (acted on by $V$) and the hole (acted on by $V^*$) by the same rotation angle. The isotropy relation (4.17) constrains the density matrix to be of the Werner form

$$\rho_{\mathrm{W}} = \frac{1}{4}(1-\xi)\mathbb{1}_4 + \xi\,|\psi_{\mathrm{Bell}}\rangle\,\langle\psi_{\mathrm{Bell}}|\,, \quad -\frac{1}{3} \leq \xi \leq 1, \qquad (4.18)$$

with $|\psi_{\text{Bell}}\rangle$ the Bell state defined in Eq. (4.12). The concurrence of the electron-hole Werner state is given by

$$C(\rho_{\text{W}}) = \frac{3}{2} \max\left(0, \xi - \frac{1}{3}\right). \qquad (4.19)$$

The parameter $\xi$ characterizing the Werner state can be calculated from

$$\xi = \text{tr}\,[(\sigma_3 \otimes \sigma_3)\rho] = \rho_{11} - \rho_{22} - \rho_{33} + \rho_{44}. \qquad (4.20)$$

Only diagonal elements of the density matrix appear in the expression (4.20) for $\xi$. These can be calculated semiclassically in the $N$-independent limit $N \gg 1$ (see Appendix 4.B), leading to the following expressions for the concurrence:

$$\langle C \rangle_{\text{diffusive}} = \begin{cases} \frac{3}{2}[\sum_{n=0}^{\infty} \xi_n]^2 - \frac{1}{2}, & 1.5\,\tau_{\text{dwell}} < \tau'_{\text{so}}, \\ 0, & 0 < \tau'_{\text{so}} < 1.5\,\tau_{\text{dwell}}, \end{cases}$$

$$\xi_n = \frac{4\pi(-1)^n(2n+1)}{\pi^2(2n+1)^2 + 8\tau_{\text{dwell}}/\tau'_{\text{so}}}, \qquad (4.21a)$$

$$\langle C \rangle_{\text{chaotic}} = \begin{cases} \frac{3}{2}(1 + \tau_{\text{dwell}}/\tau'_{\text{so}})^{-2} - \frac{1}{2}, & \frac{\tau_{\text{dwell}}}{\sqrt{3}-1} < \tau'_{\text{so}}, \\ 0, & 0 \le \tau'_{\text{so}} \le \frac{\tau_{\text{dwell}}}{\sqrt{3}-1}. \end{cases} \qquad (4.21b)$$

In Fig. 4.4 we plot the analytical result (4.21) for the concurrence. The two cases of diffusive and chaotic scattering differ only slightly. The initial slopes are the same,

$$\langle C \rangle_{\text{diffusive}} = \langle C \rangle_{\text{chaotic}} \qquad (4.22)$$
$$= 1 - 3\tau_{\text{dwell}}/\tau'_{\text{so}} + \mathcal{O}(\tau_{\text{dwell}}/\tau'_{\text{so}})^2.$$

The critical spin-orbit coupling strengths, beyond which the concurrence vanishes, are different: $\tau_{so}^{\text{critical}} = 1.5\,\tau_{\text{dwell}}$ for diffusive scattering and $\tau_{so}^{\text{critical}} = \tau_{\text{dwell}}/(\sqrt{3}-1) = 1.37\,\tau_{\text{dwell}}$ for chaotic scattering.

We also compare in Fig. 4.4 the analytical results in the chaotic case from this section with the numerical results from the previous section. The agreement is quite good for large $N$, where the semiclassical analytics is expected to hold.
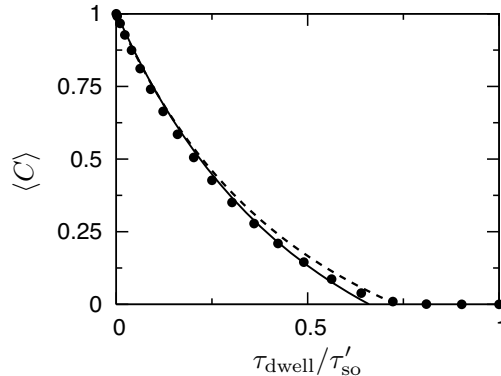
**Figure 4.4.** Ensemble averaged concurrence as a function of spin-orbit coupling rate $1/\tau'_{\mathrm{so}}$. The solid and dashed curves are the analytical results (4.21) in the case of diffusive wires and chaotic cavities, respectively, on each side of the tunnel barrier. These analytical curves use the isotropy approximation. The data points are from the numerical simulation in the chaotic case without the isotropy approximation (spin kicked rotator of Fig. 4.3, with $N = 30$).

## 4.4 Conclusion

Figure 4.4 summarizes our main findings: The effect of spin-orbit coupling on the degree of spin-entanglement of the electron-hole pairs produced at a tunnel barrier depends strongly on the ratio of the dwell time $\tau_{\mathrm{dwell}}$ and spin-orbit coupling time $\tau'_{\mathrm{so}}$. Even though $\tau_{\mathrm{dwell}}$ and $\tau'_{\mathrm{so}}$ each depend sensitively on the nature of the dynamics (diffusive or chaotic) the dependence of the concurrence on the ratio $\tau_{\mathrm{dwell}}/\tau'_{\mathrm{so}}$ is insensitive to the nature of the dynamics. The initial decay (4.22) is the same and the critical spin-orbit coupling strength (beyond which the entanglement vanishes) differs by less than 10%. This has the useful experimental implication that a single parameter suffices to quantify the amount of entanglement degradation by spin-orbit coupling.

We have tested our analytical theory using a computer simulation for the case of chaotic dynamics. (The close similarity to the diffusive results suggests that this test is representative.) Analytics and numerics are in good agreement, differing by less than 10% in the regime $N \gg 1$ of large conductance $G$ where the semiclassical analytics applies. While the semi-

classical approximation is controlled by the small parameter $1/N$ (or, more generally, $h/e^2G$), the isotropy approximation has no small parameter that controls the error. Its use is justified by the reasonable expectation that an ensemble of disordered or chaotic systems should have no preferential quantization axis for the electron and hole spins. It is gratifying to see that the numerics supports this expectation.

The standard method of experimentally verifying the presence of entanglement is by demonstrating violation of Bell inequalities. In optics this is achieved by measuring coincidence rates of photons by photodetectors (i.e. by counting photons) in different polarization bases. In the solid state one cannot simply count electrons, but rather needs to formulate the Bell inequalities in terms of correlators of spin currents (= spin noise) [84–86]. This has so far not been accomplished experimentally. Thus, the isotropy approximation that has been used here as a way to simplify the calculation of the concurrence, also has an experimental implication [87]: By relying on spin isotropy the concurrence can be obtained directly from correlators of time averaged spin currents. Our demonstration of the accuracy of the isotropy approximation may motivate experimentalists to try this "poor man's method" of entanglement detection — since average spin currents have been measured [88] while spin noise has not.

## Appendix 4.A    A Few Words on the Use of the Spin Kicked Rotator

In this chapter we have compared numerical simulations with the spin kicked rotator to analytical calculations. In order to do so, we need to know the time scales $\tau'_{\mathrm{so}}$ and $\tau_{\mathrm{dwell}}$ in the spin kicked rotator. This was implicit in our comparison with random-matrix theory in section 2.3. In this appendix we give this relation a little more explicitly.

In chapter 2 we considered Eqs. (2.32) and (2.33) as giving the relation between the model parameters of the spin kicked rotator to the physical time scale $\tau_{\mathrm{so}} = 2\tau'_{\mathrm{so}}$. One can also take these equations to define $\tau_{\mathrm{so}}$ for the model. In the spin kicked rotator $\hbar = 1$ and $\Delta = 2\pi/M$. Inserting into Eq. (2.33) and using the expression for $K_c$ from (2.32) we find the spin-orbit coupling time $\tau_{\mathrm{so}}$ (in units of the stroboscopic period) in the

model to be determined by the parameter $K_{\mathrm{so}}$ through

$$\tau_{\mathrm{so}} = 2\tau'_{\mathrm{so}} = \frac{32\pi^2}{K_{\mathrm{so}}^2 M^2}. \qquad (4.23)$$

The mean dwell time $\tau_{\mathrm{dwell}}$ (in units of the stroboscopic period) is similarly given by

$$\tau_{\mathrm{dwell}} = \frac{M}{N} = \frac{2\pi}{N\Delta}, \qquad (4.24)$$

where we have taken into account the fact that $N$ of the $2N$ channels are closed by the tunnel barrier (cf. Fig. 4.2). Notice that the mean dwell time is a classical quantity, while $N$ and $\Delta$ separately are quantum mechanical quantities.

We now use the spin kicked rotator to generate two sets scattering matrices (in our simulations we choose $K = 41$ (fully chaotic), $M = 640$, and $l_0 = 0.2$). From the reflection and transmission matrices (4.15) the density matrix (4.7) is obtained, from which the concurrence (4.13) follows. The concurrence is averaged over 20 different quasienergies $\varepsilon$, $\varepsilon'$ and over 20 different lead positions $P$, $P'$ in the two cavities (assumed to be independent scatterers). Results are shown in Fig. 4.3.

## Appendix 4.B   Calculation of Spin Correlators

The diagonal elements of the density matrix appearing in the expression (4.20) for the Werner parameter $\xi$ represent spin correlators,

$$\rho_{11} = P_{\uparrow\uparrow}, \ \rho_{22} = P_{\uparrow\downarrow}, \ \rho_{33} = P_{\downarrow\uparrow}, \ \rho_{44} = P_{\downarrow\downarrow}. \qquad (4.25)$$

Here $P_{\sigma\sigma'}$ is the probability that the outgoing electron has spin $\sigma$ and the outgoing hole has spin $\sigma'$. To calculate these correlators, it is convenient to first consider only those electrons that exit after a time $t$ and those holes that exit after a time $t'$. The time-resolved correlator $P_{\sigma\sigma'}(t,t')$ gives the desired $P_{\sigma\sigma'}$ after integration over time,

$$P_{\sigma\sigma'} = \int_0^\infty dt \int_0^\infty dt' P_{\sigma\sigma'}(t,t') P_{\mathrm{dwell}}(t) P_{\mathrm{dwell}}(t'), \qquad (4.26)$$

weighted by the dwell time distribution $P_{\text{dwell}}$ (we assume that the dwell times at the left and right of the tunnel barrier are independent and identically distributed).

As initial condition we take

$$P_{\sigma\sigma'}(0,0) = \frac{1}{2}\delta_{\sigma\sigma'}, \qquad (4.27)$$

corresponding to the spin state immediately after the tunnel event. Spin-orbit coupling randomizes the spin with a rate $1/\tau'_{\text{so}}$, so that $P_{\sigma\sigma'}(t,t')$ decreases in time according to the rate equations

$$\frac{d}{dt}P_{\sigma\sigma'}(t,t') = \frac{1}{2\tau'_{\text{so}}}\sum_{\sigma''}[P_{\sigma''\sigma'}(t,t') - P_{\sigma\sigma'}(t,t')], \qquad (4.28a)$$

$$\frac{d}{dt'}P_{\sigma\sigma'}(t,t') = \frac{1}{2\tau'_{\text{so}}}\sum_{\sigma''}[P_{\sigma\sigma''}(t,t') - P_{\sigma\sigma'}(t,t')]. \qquad (4.28b)$$

The solution of the rate equations (4.28) with the initial condition (4.27) is

$$P_{\uparrow\uparrow}(t,t') = P_{\downarrow\downarrow}(t,t') = \frac{1}{4} + \frac{1}{4}e^{-(t+t')/\tau'_{\text{so}}}, \qquad (4.29a)$$

$$P_{\uparrow\downarrow}(t,t') = P_{\downarrow\uparrow}(t,t') = \frac{1}{4} - \frac{1}{4}e^{-(t+t')/\tau'_{\text{so}}}. \qquad (4.29b)$$

To complete the calculation we need the dwell time distribution. For a chaotic cavity this has the well known exponential form [89]

$$P_{\text{dwell,chaotic}} = \frac{1}{\tau_{\text{dwell}}}e^{-t/\tau_{\text{dwell}}}, \qquad (4.30)$$

with

$$\tau_{\text{dwell}} = \frac{2\pi\hbar}{N\Delta} \qquad (4.31)$$

inversely proportional to the mean level spacing $\Delta$ of Kramers degenerate levels in the cavity.

For the diffusive wire (diffusion constant $D$) we determine $P_{\text{dwell}}$ by
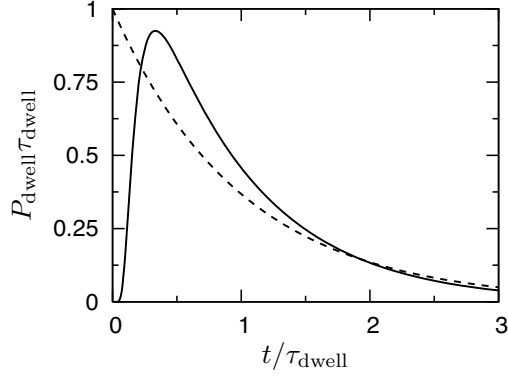
**Figure 4.5.** Dwell time distribution in a diffusive wire (solid line) and chaotic cavity (dashed line).

solving the one-dimensional diffusion equation

$$\left(\frac{\partial}{\partial t} - D\frac{\partial^2}{\partial x^2}\right)p(x,t) = 0, \quad 0 < x < L, \tag{4.32}$$

with initial and boundary conditions

$$\frac{\partial p}{\partial x}(0,t) = 0, \quad p(L,t) = 0, \quad p(x,0) = \delta(x). \tag{4.33}$$

Here $p(x,t)$ is the classical probability of finding a particle at point $x$ at time $t$. The boundary conditions represent reflection by the high tunnel barrier at $x = 0$ and absorption by the reservoir at $x = L$.

The probability that the particle is still in the wire at time $t$ is given by

$$N(t) = \int_0^L p(x,t)dx, \tag{4.34}$$

and therefore the dwell time distribution is

$$P_{\text{dwell}} = -\frac{dN(t)}{dt}. \tag{4.35}$$

Solution of the diffusion equation by expansion in eigenstates gives the

result in the form

$$P_{\text{dwell, diffusive}} = \frac{\pi}{2\tau_{\text{dwell}}} \sum_{n=0}^{\infty} (-1)^n (2n+1) e^{-(2n+1)^2 \frac{\pi^2}{8} \frac{t}{\tau_{\text{dwell}}}}. \qquad (4.36)$$

The mean dwell time is

$$\tau_{\text{dwell}} = \frac{L^2}{2D}. \qquad (4.37)$$

The dwell time distributions for the chaotic and diffusive dynamics are compared in Fig. 4.5.

Collecting results we arrive at the expressions (4.21) for the concurrence given in the main text.